The Cryosphere Discuss., 8, 5623–5644, 2014
www.the-cryosphere-discuss.net/8/5623/2014/
doi:10.5194/tcd-8-5623-2014

The Cryosphere Discussions
Open Access

Snow mass decrease in the Northern Hemisphere (1979/80–2010/11)

Z. Li[1], J. Liu[1,2], L. Huang[1], N. Wang[3], B. Tian[1], J. Zhou[1], Q. Chen[1], and P. Zhang[1]

[1]Key Laboratory of Digital Earth Science, Institute of Remote Sensing and Digital Earth, Chinese Academy of Sciences, Beijing, 10094, China
[2]Graduate University of Chinese Academy of Sciences, Beijing, 100049, China
[3]Cold and Arid Regions Environmental and Engineering Research Institute, Chinese Academy of Sciences, Lanzhou, 730000, China

Received: 19 September 2014 – Accepted: 15 October 2014 – Published: 6 November 2014

Correspondence to: Z. Li (lizhen@radi.ac.cn) and L. Huang (huanglei@radi.ac.cn)

Published by Copernicus Publications on behalf of the European Geosciences Union.

Snow mass decrease in the Northern Hemisphere (1979/80–2010/11)

Z. Li et al.

Abstract

Snow cover has a key effect on climate change and hydrological cycling, as well as water supply to a sixth of the world's population across the Northern Hemisphere. However, reliable data on trends in snow cover in the Northern Hemisphere is lacking. Snow water equivalent (SWE) is a common measure of the amount of equivalent water of the snow pack. Here we verify the accuracy of three existing global SWE products and merge the most accurate aspects of them to generate a new SWE product covering the last 32 years (1979/80–2010/11). Using this new SWE product, we show that there has been a significant decreasing trend in the total mass of snow in the Northern Hemisphere. The most notable changes in total snow mass are -16.45 ± 6.68 and -13.55 ± 7.80 Gt year^{-1} in January and February, respectively. These are followed by March and December, which have trends of -12.58 ± 6.88 and -10.70 ± 5.62 Gt year^{-1}, respectively, from 1979/80 to 2010/11. During the same period, the temperature in the study area raised 0.17 °C decade^{-1}, which is thought to be the main reason of SWE decline.

1 Introduction

The world's snow cover is concentrated in the Northern Hemisphere and plays a crucial role in climate change and regional water supply (Pardé et al., 2007; Takala et al., 2011; Barnett et al., 2005; Hancock et al., 2013; Immerzeel et al., 2010). Snow cover extent (SCE) shrank over the Northern Hemisphere between the 1970s and 2006 (Karl et al., 1993; Gao et al., 2012; Déry and Brown, 2007; Armstrong and Brodzik, 2001). Snow water equivalent (SWE) is a more comprehensive parameter that takes into account snow extent, density and depth, and represents the corresponding depth of water that would result were the snow to melt in place. The pan-Arctic average trend in peak seasonal SWE was -0.17 cm decade^{-1}, with maximum and minimum trends of 5.70 and -2.5 cm decade^{-1}, respectively, for the period 1979–2009 (Liston and Hiemstra, 2011). However, the variation in SWE differed according to location and time. During the period covering the last 30 years and more, three passive microwave radiometers have been used to generate the SWE data. The products that have been used to estimate the SWE at the scale of the Northern Hemisphere consist of:

1. "Global Monthly EASE-Grid Snow Water Equivalent Climatology" product, which covers the period from November 1978 to May 2007 (Armstrong et al., 2007). The passive radiometers used to produce this were the Scanning Multichannel Microwave Radiometer (SMMR) and selected Special Sensor Microwave/Imagers (SSM/I). The AMSR-E L3 Global SWE product, which covers the period June 2002 to October 2011 (Tedesco et al., 2004; Chang et al.,1987; Armstrong and Brodzik, 2001). Both the two products are released by the National Snow and Ice Data Center (NSIDC).

2. The GlobSnow SWE product (v1.3), covering the period from 1978 to the present (Takala et al., 2011; Pulliainen, 2006; Takala et al., 2009), which is released by the European Space Agency (ESA).

Due to their different inversion algorithms, the three SWE products have different estimated accuracies and no comparison between them, or error analysis for them, has been produced at the scale of the Northern Hemisphere during their period of operation.

2 Methods

2.1 Data preprocessing

SMMR and SSM/I are passive radiometers and their brightness temperatures at frequencies of 18(19) and 37 GHz are employed to estimate SWE. In the inversion algorithm, two important approximations have been made: firstly, the snow grain size is assumed to be a constant 0.3 mm; secondly, snow density is set to a constant 0.3 g cm^{-3}

(Tedesco and Narvekar, 2010). This data set is projected on to the Equal Area Scalable Earth Grid (EASE-grid) at the hemisphere scale. Pixels from the 25 km EASE-Grid version of the BU-MODIS Land Cover data that had more than 50 % ice cover were set as permanent ice (ice sheets, ice shelves, and large glaciers) and without SWE inversion values. As any vegetation scatters microwaves in the same way as snow, the presence of vegetation will affect the SWE estimates. Therefore, pixels covered by forest were adjusted using the forest fraction.

The AMSR-E L3 Global SWE is also projected on to a 25 km × 25 km EASE-grid on the hemisphere scale. The algorithm used to produce this product is derived from the spectral difference method and is similar to the Global Monthly SWE Product of SMMR & SSM/I. With the availability of the special X-band channels on AMSR-E at 10.7 GHz, the algorithm's ability to detect deep snow (using the difference between 10.7 and 18.7 GHz) is improved and its dynamic range to help with forest attenuation is enhanced (Tedesco and Narvekar, 2010). Before the SWE values can be retrieved, wet snow pixels have to be excluded. The forest effect is corrected with the IGBP (International Geosphere Biosphere Programme) data obtained from the Boston University. It should be noted that the snow density employed in the AMSR-E L3 product is no longer a constant; instead, its value is obtained from a global snow density map, in which the average snow density values for each of the six seasonal classes (Sturm and Holmgren, 1995) are calculated according to in situ measurements made in Canada (Brown and Braaten, 1998) and the former Soviet Union (Krenke, 2004). In addition, the land cover, ocean, and ice-sheet masks are based on the MOD12Q1 data, re-gridded as a 25 km EASE-Grid version of the land cover data (MOD12Q1 IGBP, collection V004). The method of defining "ice" pixels is the same as for the SMMR & SSM/I Global Monthly SWE product discussed earlier.

The GlobSnow SWE product is retrieved using an assimilation scheme based on a semi-empirical snow emission model from satellite data combined with ground-based weather station measurements and covers all land surface areas except for mountainous regions and Greenland. The data are stored in the EASE-Grid format. The snow density is treated as a constant with a value of $0.24\,g\,cm^{-3}$, a reasonable "global" value given by the analysis by Sturm (2010). This inversion algorithm is developed further and is fully described in the article by Pulliainen et al. (2006), where considerations of the temporal continuity of the SWE are added. The mountain mask applied is derived from a $2' \times 2'$ grid of ETOP2 data containing global elevation and bathymetry from the National Geophysical Data Center (NGDC). Due to the saturated brightness temperature response, wet snow or temporary thin snow layers are not reliably detected and are masked by observed brightness temperature values using an empirical equation.

2.2 Ground station data validation

We selected coarse snow depth measurements from 7388 weather stations (Fig. 1) – each of them with at least 15 days' snow cover – from Global Historical Climatology Network-Daily (GHCN-DAILY) to be used as ground truth data, in order to validate monthly SWE estimate products. Accumulations are displayed in 5 mm steps in Fig. 2, in order to show the trends more clearly. The results of the comparison, used as ground truth for SWE values between 0 and 200 mm (Fig. 2), suggest that in the Northern Hemisphere, for values of SWE over 30 mm, the linear relationship between the estimated GlobSnow SWE and the ground truth SWE is better than for the SWE products released by the NSIDC. For GlobSnow the correlation index is over 0.5, while for the other products the correlation indexes are only 0.22 and 0.12. This is largely because a large number of in situ measurements of snow depth have been introduced into GlobSnow's inversion algorithm and improved its accuracy (Luojus et al., 2010). However, since the microwave upwelling radiation emitted from the ground by scattering no longer decreases with increasing snow depth at higher frequency microwaves (such as 37 GHz), passive microwave SWE retrieval algorithms do not have the ability to detect deep snow. The assimilation retrieval process of GlobSnow is also influenced by this limitation. In previous studies, the observable scattering at higher frequencies saturates for thick snow packs after a certain threshold, often between 120 and 180 mm.

While SWE values exceed the threshold, the accuracy of all the inversion procedures drops sharply, as the situations shown in Fig. 2.

Note that for thin snow – that is for values of SWE less than 30 mm (equivalent to a snow depth of 12 cm for a snow density of 0.24 g cm^{-3}, and a snow depth of less than 10 cm for a snow density of 0.3 g cm^{-3}) – the GlobSnow SWE values are clearly overestimates, which is the same as the result obtained from the accuracy testing experiments for Eurasia (Luojus et al., 2010).

2.3 Data merge

According to the results of comparing the three estimated SWE products and the station measurements, it was seen that for SWE > 30 mm, the GlobSnow product is more accurate than products produced by the NSIDC and that for SWE < 30 mm, the situation is reversed. In order to optimize the SWE dataset, we chose pixels that had monthly SWE values continuous above 30 mm in winter (December to March) for the period 1979/80 to 2010/11 from GlobSnow, and the other pixels that had monthly SWE values no more than 30 mm in the same period from the two NSIDC products. However, the period covered by the sets of pixels from the two NSIDC products is different: SMMR & SSM/I end in May 2007, whereas the AMSR-E data cover the period from June 2002 to October 2011. We built linear fitting equations for each pixel in every month during the period of overlap (2002–2007) in order to simulate winter SWEs in 2007–2011 using AMSR-E products. For each pixel,

$$SWE'_{ij,\mathrm{mon}} = \alpha SWE_{ij,\mathrm{mon}} + \beta \quad (1)$$

where SWE′ is obtained from NSIDC SWE products derived from SSMR & SMM/I data at location (i, j) in one of the winter months and SWE is obtained from the NSIDC SWE product derived from AMSR-E data, α and β are linear coefficient. Considering the differences in the algorithms used to produce these products, this kind of forecasting is not effective in all areas. Simulated data was added only for pixels that proved to be

TCD
8, 5623–5644, 2014

statistically significant at $p = 0.05$ under both a t test and an F test. For the remainder, the SWE series from SSMR & SMM/I (ending in 2007) was retained in the pixels and the simulated data is not added, in order to avoid the introduction of errors into the trend analysis. However, in the calculation of the total snow mass, the values of SWE in the non-simulated pixels were still replaced by those from the NSIDC AMSR-E product as the low number of small values has relatively little influence.

In the merged products, the distribution maps of the three different products are shown in Fig. 3. The GlobSnow product accounts for the largest proportion (more than 50 %) in the merged data in all the four months, and it mainly concentrates in high altitude regions. The NSIDC (SMMR & SSM/I and the linear fitted AMSR-E) product accounts for a little larger proportion than the NSIDC (SMMR/SSM/I) product in all the four months except in February, and both of the two products mainly distributed in low altitude regions.

3 Results

The distribution map of the average optimized SWE product for the 32 years is presented in Fig. 4. In December, snow cover is mainly located between 55 and 70° N in Eurasia and between 60–70° N in North America. Snow cover extends to mid-latitude regions near 50° N in January in Eurasia and North America, and there is little difference between January, February and March in these areas. Large areas in central and western Siberia have the biggest and deepest snow accumulations of snow in all four months.

Using the optimized SWE product (1979/80–2010/11), and the trend-free pre-whitening Mann–Kendall (TFPW-MK) (Yue et al., 2002) method, which has been widely used for hydro-meteorological trend assessments (Gao et al., 2012), we analyzed the SWE changes in the past 32 years in the Northern Hemisphere for different regions and different months, as shown in Fig. 5.

TCD
8, 5623–5644, 2014

According to the SWE change map (Fig. 5), in December, there was a significant change in central Siberia (60–70° N, 110–130° E) of about −1 cm decade^{-1}. Over the West Siberian Plain and parts of the Eurasian continent near 60° N there was a slight increase, but the most significant rise was concentrated around 66° N, 90° E – the rate of increase here was over 1 cm decade^{-1}. In January, the area where there was a significant decrease in SWE increases several fold, and is not only concentrated in the same regions as December but also extends to Baffin Island and northern Europe. In February, the rate of SWE decrease in Siberia accelerates, reaching over −2 cm decade^{-1}; the areas where there is a decrease also grows further to include most of the Hudson Bay coastline. Meanwhile, the rising trend around 60° N in Siberia weakens, with the maximum rate being 0.7 cm decade^{-1}. In March, the significant reduction in SWE in North America is still obvious even though the pattern is variable with some small areas where there is an increase. In Northern Europe, there is a reduction in the area where there is a significant decrease, whereas there is a clear expansion in areas where there is an increase and this area of increase extends to the Eastern European Plain.

Overall, then, significant drops in SWE are concentrated at high latitudes of around 65° N in Siberia and in North America; areas where there was a rise are mainly scattered around 60° N in Eurasia. In Eurasia there was a significant decline in SWE in northern areas but an increasing trend in areas towards the south of the snow-covered areas, except for the "edges" of the snow-covered area below approximately 58° N. In North America the overall SWE declined and significant changes are concentrated along the coast of Hudson Bay and parts of Alaska in January and February.

From the temporal view, although the monthly total snow mass fluctuates from year to year, there is a declining trend in the Northern Hemisphere for all winter months in the period 1979/80–2010/11 (Fig. 6). The monthly total snow mass is calculated by summing the total mass of snow in all pixels. The most serious snow mass change occurred in January and February, at rates of −16.45 ± 6.68 and −13.55 ± 7.80 Gt year^{-1}, respectively, corresponding to −0.67 and −0.45 % per year, whereas the rate in March was −12.58 ± 6.88 Gt year^{-1}, or nearly −0.42 % per year. The smallest change was in

TCD
8, 5623–5644, 2014

December – only -10.70 ± 5.62 Gt year^{-1}, taking up to a change rate of -0.64 % per year. There is high confidence in these monthly total snow mass changes (significance level $p < 0.01$). From the perspective of monthly differences, at less than 2000 Gt the total snow mass in December is the lowest for the four winter months; the value increases to about 2500 Gt in January, and reaches a peak of about 3000 Gt in February, with this value lasting into March.

Focusing on the more recent 15 years from 1996/97 to 2010/11, we found that the rate of decrease in the SWE slows down for the four months studied except in March, and the trend becomes less significant. During this period, the changing rate was -9.08 ± 6.90 Gt year^{-1} in December, -13.15 ± 8.74 Gt year^{-1} in January and -10.87 ± 10.56 Gt year^{-1} in February ($p < 0.1$). It should be noted that the February results are not statistically significant. In March the rate accelerated to -13.16 ± 6.6 Gt year^{-1} ($p < 0.1$).

To validate the results of this work, the results of the merged data are compared with the SWE changes in North America (Gan et al., 2013) which uses the SSMR and SSM/I data only, as shown in Fig. 7. Both Gan et al.'s (2013) and our results use the Mann–Kendall trend analysis method, which guarantees the differences are caused by the data source only. In the comparison, both the two data sets show decreasing trend in the studied four months, but in different decreasing rate. Compared to the results of Gan et al., the decreasing rate acquired from the merged data is faster in December and January, but slower in February and March.

4 Discussions

4.1 Accuracy analysis

Due to different data sources and different processing procedures, the existing three SWE products may differ greatly in different regions (Liu et al., 2014). The accuracy of the three existing SWE products is tested with ground station data in the Northern

TCD
8, 5623–5644, 2014

Hemisphere, and the 30 mm threshold is acquired. Theoretically, the fusion of the GlobSnow products thicker than 30 mm and the NSIDC products thinner than 30 mm is the best choice. However, it should be noted that, the conclusion is based on about 30 years ground station validation in the whole Northern Hemisphere, so it is only a statistical result. The merged product is superior in the Northern Hemisphere for the past 30 years, and it is more suitable for total SWE or average SWE calculation in the whole Northern Hemisphere, but it is not necessary the most accurate choice for a certain region or a certain time.

4.2 Relation to climate changes

As a feature that is responsive to climate change, SWE is affected by changes in air temperature and also by changes in precipitation timing and seasonality (Immerzeel et al., 2010). To find out the relation between changes in the value of SWE and climate change, we collected the global monthly gridded datasets of air temperature and precipitation, and analyzed the trends in these data for the past 32 years. Snowfall and rainfall cannot be separated in the precipitation records; however, the study areas used in this work are mostly at latitudes higher than 50° N and so all the precipitation in the four months being considered was treated as snow.

The average winter temperature and precipitation changes in the snow-covered areas found using the TFPW-MK method are shown in Fig. 8. In the past 32 years, the temperature has increased at a rate of 0.17 °C decade^{-1} and the precipitation increased at a rate of 0.4 mm decade^{-1}.

On a global scale, most climate data and models agree that there is a near-surface warming trend due to the rising levels of greenhouse gases in the atmosphere (Barnett et al., 2005). According to the fifth IPCC report (IPCC, 2013), the global warming rate over the past 15 years (1998–2012) has been 0.05 (−0.05 to +0.15) °C decade^{-1} and for the period since 1951 (1951–2012) the rate is calculated as 0.12 (0.08 to 0.14) °C decade^{-1}. In a warmer world, the melting and sublimating of winter snow

TCD
8, 5623–5644, 2014

accelerates (Cox et al., 2000). Even though the precipitation is also increasing, the total snow mass on the ground decreased.

The decrease in SWE directly reduces water supply in the spring (Barnett et al., 2005; Diffenbaugh et al., 2012) and also influences vegetation growth (Wahrent et al., 2005; Wang et al., 2013). In addition, it has a complex influence on the ground climate. On the one hand, the snowpack insulates soil from cold air so the thinning of the snow weakens the insulating effect and cools the soil (Zhang et al., 2005) in winter; on the other hand, thinning of the snow is positively related with snow-season shortening and soil without snow cover absorbs more solar energy and warms up in spring (Lawrence et al., 2010).

5 Conclusions

Three SWE products, NSIDC (SSMR & SSMI), NSIDC (AMSR-E L3) and GlobSnow are verified using global weather station data. The results show that for values of SWE less than 30 mm, the NSIDC product has the best correlation with the ground truth data; when the SWE is between 30 and 200 mm, the GlobSnow product shows the best correlation. Based on the validation results, we choose pixels (of size 25 km × 25 km) that have monthly SWE values above 30 mm in the GlobSnow SWE product for the period 1979/80–2010/11 and the remaining pixels from the NSIDC products to optimize the SWE product.

Using this new SWE product, we show that, although the snow mass fluctuates from year to year, there has been a significant decreasing trend in the total mass of snow in the Northern Hemisphere for the period 1979/80–2010/11. The most notable declines in total snow mass are -16.45 ± 6.68 and -13.55 ± 7.80 Gt year^{-1} in January and February, respectively. These are followed by March and December, which have decreasing trends of -12.58 ± 6.88 and -10.70 ± 5.62 Gt year^{-1}, respectively, from 1979/80 to 2010/11. The most significant decline is concentrated between 65 and 75° N in Siberia and North America; in contrast, there has been an increase in snow mass at latitudes near 60° N in Eurasia. Both the temperature and precipitation increased in the study area, but the temperature rise is speculated to play a more important on snow cover.

Acknowledgements. This research was supported by the Chinese Ministry of Science and Technology (grant numbers 2010CB951403, and 2011AA120403). The NSIDC (SSMR & SSM/I) and NSIDC (AMER-E) SWE data for this paper are available at the National Snow and Ice Data Center (NSIDC). GlobSnow SWE data is provided by European Space Agency (ESA). Temperature and precipitation data are provided by National Oceanic and Atmospheric Administration (NOAA).

References

Armstrong, R. L. and Brodzik, M. J.: Recent Northern Hemisphere snow extent: a comparison of data derived from visible and microwave satellite sensors, Geophys. Res. Lett., 28, 3673–3676, 2001.

Armstrong, R. L., Brodzik, M. J., Knowles, K., and Savoie, M.: Global Monthly EASE-Grid Snow Water Equilivalent Climatology, National Snow and Ice Data Center, Boulder, Colorado, USA, 2007.

Barnett, T. P., Adam, J. C., and Lettenmaier, D. P.: Potential impacts of a warming climate on water availability in snow-dominated regions, Nature, 438, 303–309, 2005.

Brown, R. D. and Braaten, R. O.: Spatial and temporal variability of Canadian monthly snow depths, 1946–1995, Atmos. Ocean, 36, 37–54, 1998.

Chang, A., Foster, J., and Hall, D.: Nimbus-7 SMMR derived global snow cover parameters, Ann. Glaciol., 9, 39–44, 1987.

Cox, P. M., Betts, R. A., Jones, C. D., Spall, S. A., and Totterdell, I. J.: Acceleration of global warming due to carbon-cycle feedbacks in a coupled climate model, Nature, 408, 184–187, 2000.

Déry, S. J. and Brown, R. D.: Recent Northern Hemisphere snow cover extent trends and implications for the snow-albedo feedback, Geophys. Res. Lett., 34, L22504, doi:10.1029/2007GL031474, 2007.

Diffenbaugh, N., Scherer, M., and Ashfaq, M.: Response of snow-dependent hydrologic extremes to continued global warming, Nat. Clim. Change, 3, 379–384, 2012.

Gao, J., Williams, M. W., Fu, X., Wang, G., and Gong, T.: Spatiotemporal distribution of snow in eastern Tibet and the response to climate change, Remote Sens. Environ., 121, 1–9, 2012.

Gan, T., Barry, R., Gizaw, M., Gobena, A., and Balaji, R.: Changes in North American snowpacks for 1979–2007 detected from the snow water equivalent data of SMMR and SSM/I passive microwave and related climatic factors, J. Geophys. Res., 118, 7682–7697, 2013.

Hancock, S., Baxter, R., Evans, J., and Huntley, B.: Evaluating global snow water equivalent products for testing land surface models, Remote Sens. Environ., 128, 107–117, 2013.

Immerzeel, W. W., van Beek, L. P., and Bierkens, M. F.: Climate change will affect the Asian water towers, Science, 328, 1382–1385, 2010.

IPCC: Working Group 1 Contribution to the IPCC Fifth Assessment Report, Climate Change 2013: The Physical Science Basis, Summary for Policymakers, IPCC WGI AR5, Cambridge University Press, Cambridge and New York, 2013.

Karl, T. R., Groisman, P. Y., Knight, R. W., and Heim Jr., R. R.: Recent variations of snow cover and snowfall in North America and their relation to precipitation and temperature variations, J. Climate, 6, 1327–1344, 1993.

Krenke, A.: Former Soviet Union Hydrological Snow Surveys, 1966–1996, National Snow and Ice Data Center/World Data Center for Glaciology, Boulder, 2004.

Lawrence, D. M. and Slater, A. G.: The contribution of snow condition trends to future ground climate, Clim. Dynam., 34, 969–981, 2010.

Liston, G. E. and Hiemstra, C. A.: The changing cryosphere: pan-Arctic snow trends (1979–2009), J. Climate, 24, 5691–5712, 2011.

Liu, J. Li, Zh., Huang, L., and Tian, B.: Hemispheric-scale comparison of monthly passive microwave snow water equivalent products, J. Appl. Remote Sens., 8, 1–16, doi:10.1117/1.JRS.8.084688, 2014.

Luojus, K., Pulliainen, J., Takala, M., Derksen, C., Rott, H., Nagler, T., Solberg, R., Wiesmann, A., Metsamaki, S., Malnes, E., and Bojkov, B.: Investigating the feasibility of the globsnow snow water equivalent data for climate research, IGARSS, Honolulu, 4851–4853, 2010.

Pardé, M., Goïta, K., and Royer, A.: Inversion of a passive microwave snow emission model for water equivalent estimation using airborne and satellite data, Remote Sens. Environ., 111, 346–356, 2007.

Pulliainen, J.: Mapping of snow water equivalent and snow depth in boreal and sub-arctic zones by assimilating space-borne microwave radiometer data and ground-based observations, Remote Sens. Environ., 101, 257–269, 2006.

Sturm, M., Taras, B., Liston, G. E., Derksen, C., Jonas, T., and Lea, J.: Estimating snow water equivalent using snow depth data and climate classes, J. Hydrometeorol., 11, 1380–1394, 2010.

Takala, M., Pulliainen, J., Metsamaki, S. J., and Koskinen, J. T.: Detection of snowmelt using spaceborne microwave radiometer data in Eurasia from 1979 to 2007, IEEE T. Geosci. Remote, 47, 2996–3007, 2009.

Takala, M., Luojus, K., Pulliainen, J., Derksen, C., Lemmetyinen, J., Kärnä, J., Koskinen, J., and Bojkov, B.: Estimating Northern Hemisphere snow water equivalent for climate research through assimilation of space-borne radiometer data and ground-based measurements, Remote Sens. Environ., 115, 3517–3529, 2011.

Tedesco, M. and Narvekar, P. S.: Assessment of the NASA AMSR-E SWE Product, IEEE J. Sel. Top. Appl., 3, 141–159, 2010.

Tedesco, M., Kelly, R., Foster, J. L., and Chang, A. T. C.: AMSR-E/Aqua Daily L3 Global Snow Water Equivalent EASE-Grids V002, NASA DAAC at the National Snow and Ice Data Center, Boulder, Colorado, USA, 2004.

Sturm, M., Holmgren, J., and Liston, G. E.: A seasonal snow cover classification system for local to global applications, J. Climate, 8, 1261–1283, 1995.

Wahrent, C.-H. A., Walker, M. D., and Bret-Harte, M. S.: Vegetation responses in Alaskan arctic tundra after 8 years of a summer warming and winter snow manipulation experiment, Glob. Change Biol., 11, 537–552, 2005.

Wang, K., Zhang, L., Qiu, Y., Ji, L., Tian, F., Wang, C., and Wang, Z.: Snow effects on alpine vegetation in the Qinghai-Tibetan Plateau, Int. J. Digit. Earth, doi:10.1080/17538947.2013.848946, online first, 2013.

Yue, S., Pilon, P., Phinney, B., and Cavadias, G.: The influence of autocorrelation on the ability to detect trend in hydrological series, Hydrol. Process., 16, 1807–1829, 2002.

Zhang, T.: Influence of the seasonal snow cover on the ground thermal regime: an overview, Rev. Geophys., 43, doi:10.1029/2004RG000157, online first, 2005.

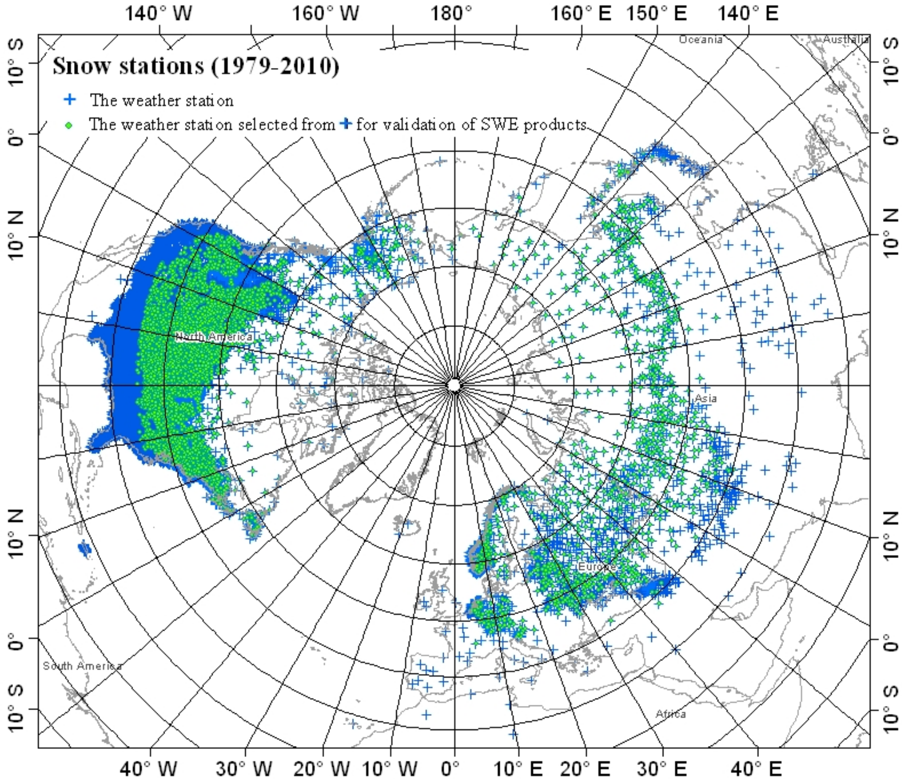

Figure 1. Ground station distribution. The crosses stand for 29 814 stations that provide snow depth measurements for 1979–2010. The points stand for 7388 selected stations – at each of these, there were at least 15 days of snow cover in the month studied and the stations used in the assimilation algorithm of the GlobSnow product were eliminated.

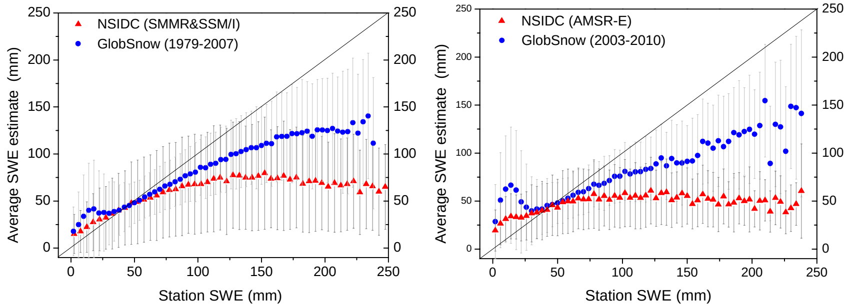

	0<SWE < 30mm			30mm <SWE <200mm		
	Corr.coeff	RMSE/mm	bias/mm	Corr.coeff	RMSE/mm	bias/mm
NSIDC(SMMR&SSM/I)	0.28	21.07	10.97	0.22	34.37	-22.41
GlobSnow (1979-2007)	0.21	29.13	25.15	0.63	22.59	-8.65
NSIDC(AMSR-E)	0.27	18.35	17.58	0.12	19.26	-11.24
GlobSnow (2003-2010)	0.09	30.68	43.18	0.55	19.33	-16.35

Figure 2. Comparation between ground truth station snow water equivalent (SWE) and derived SWE estimates.

TCD
8, 5623–5644, 2014

Snow mass decrease in the Northern Hemisphere (1979/80–2010/11)

Z. Li et al.

Title Page
Abstract Introduction
Conclusions References
Tables Figures
◀ ▶
Back Close
Full Screen / Esc
Printer-friendly Version
Interactive Discussion

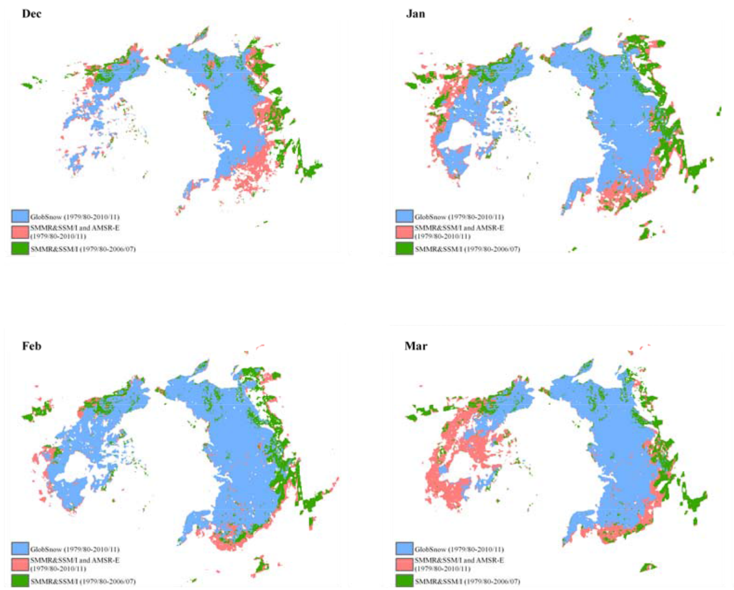

SWE Products	Percentage of the total area of the merged SWE products (%)			
	Dec	Jan	Feb	Mar
GlobSnow (1979-2011)	59.21	61.26	70.50	56.92
NSIDC(SMMR&SSM/I) and the linear fitted AMSR-E (1979-2011)	24.18	19.44	12.08	26.92
NSIDC(SMMR&SMM/I) (1979-2007)	16.61	19.30	17.42	16.16
Total	100	100	100	100

Figure 3. The distribution and contribution of different SWE procudts in the merged data.

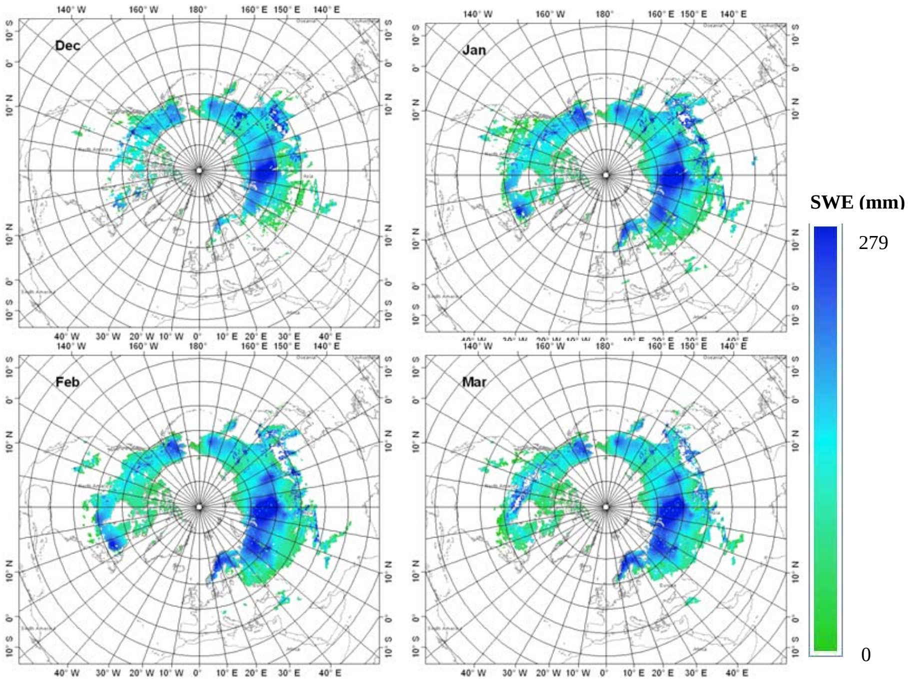

Figure 4. The average SWE distribution map in the Northern Hemisphere from 1979/80 to 2010/11.

TCD

8, 5623–5644, 2014

Snow mass decrease in the Northern Hemisphere (1979/80–2010/11)

Z. Li et al.

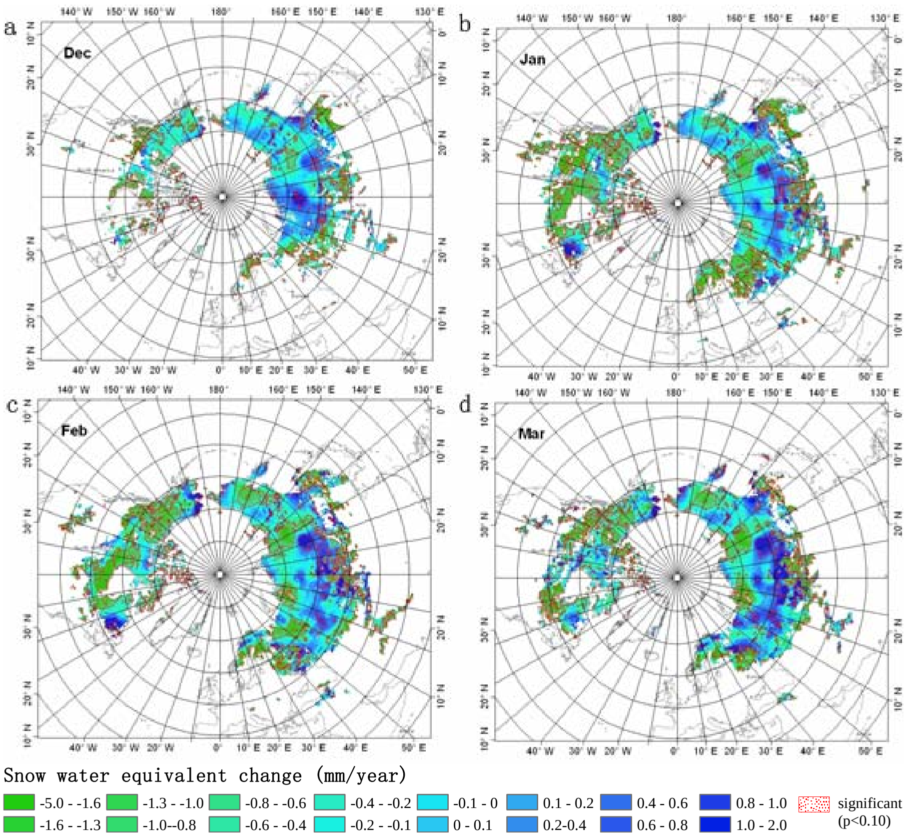

Figure 5. Changes in Northern Hemisphere monthly SWE in winter (1979/80–2010/11). **(a)** SWE changes in December. **(b)** SWE changes in January. **(c)** SWE changes in February. **(d)** SWE changes in March.

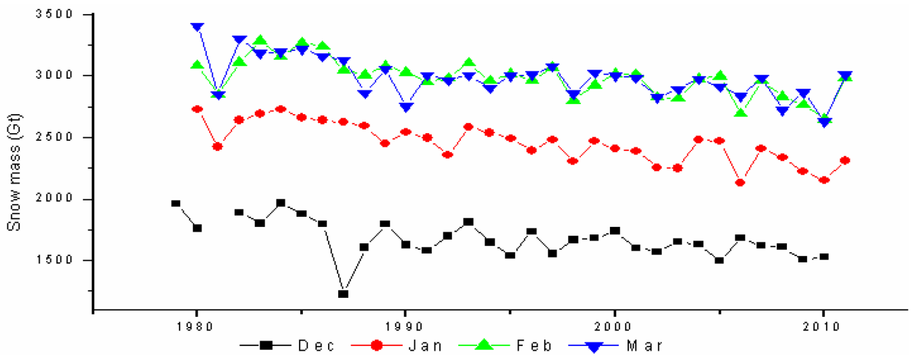

Figure 6. Variations in the total snow mass in the Northern Hemisphere in winter for the period 1979/80–2010/11.

TCD
8, 5623–5644, 2014

Snow mass decrease in the Northern Hemisphere (1979/80–2010/11)

Z. Li et al.

Title Page
Abstract | Introduction
Conclusions | References
Tables | Figures
◄| |►
◄ ►
Back | Close
Full Screen / Esc
Printer-friendly Version
Interactive Discussion

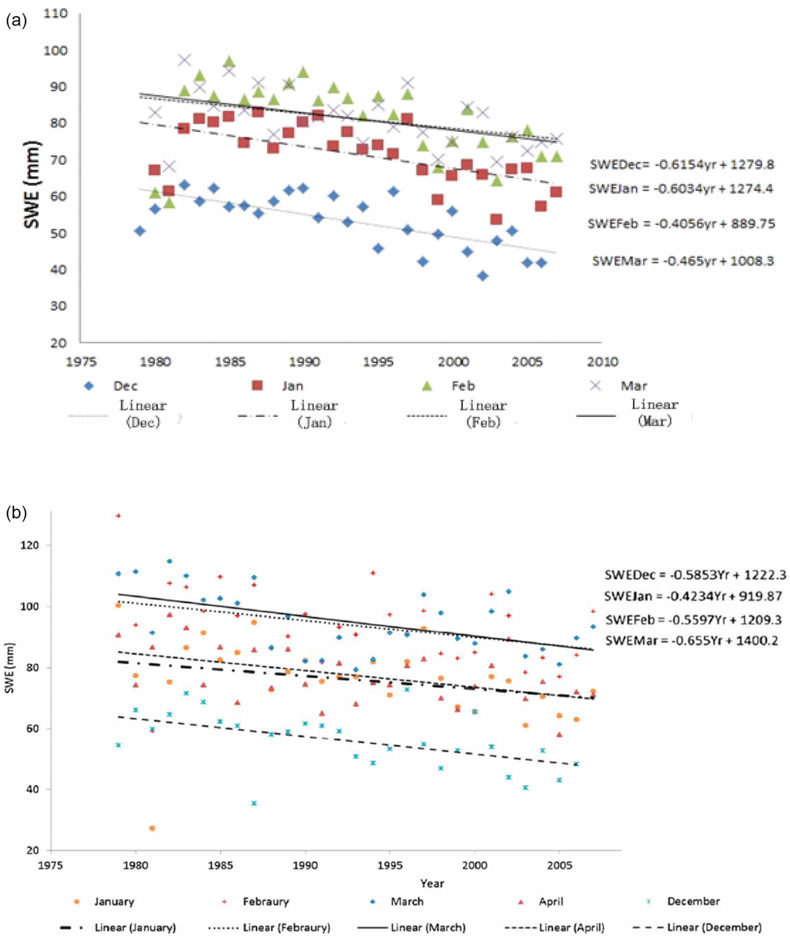

Figure 7. Comparison of the SWE change using the merged data **(a)** and the SSMR and SSM/I data **(b)** (Gan et al., 2013).

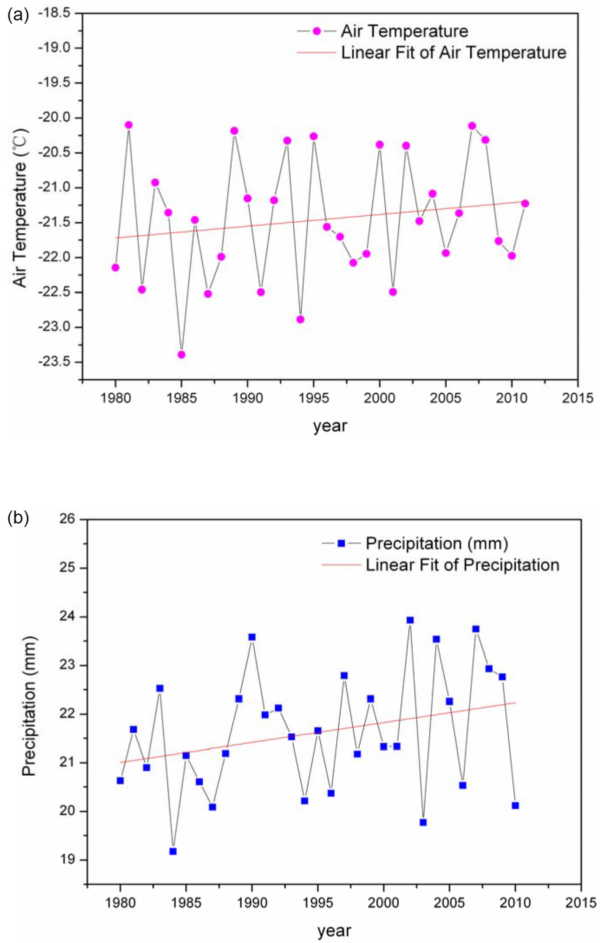

Figure 8. (a) The average winter temperature change in the snow-covered areas, **(b)** the average monthly winter precipitation change in the snow covered areas.

TCD
8, 5623–5644, 2014